Asian Journal of Water, Environment and Pollution. Vol. 22, No. 4 (2025), pp. 187-204.
doi: 10.36922/AJWEP025240191

ORIGINAL RESEARCH ARTICLE

Tailored Bombax ceiba-based activated carbons for enhanced rhodamine B removal: A sustainable approach to industrial effluent remediation

Dibyashree Shrestha*

Department of Chemistry, Institute of Science and Technology, Patan Multiple Campus, Tribhuvan University, Lalitpur, Bagmati, Nepal

***Corresponding author:** Dibyashree Shrestha (shresthadibyashree@gmail.com)

Received: June 9, 2025; 1st revised: July 1, 2025; 2nd revised: July 3, 2025; Accepted: July 7, 2025; Published online: July 28, 2025

Abstract: *Bombax ceiba* wood waste-derived activated carbon (AC) provides a low-cost, sustainable, and efficient solution for rhodamine B (RhB) dye removal from industrial wastewater through eco-friendly adsorption techniques. This study reports the synthesis of ACs from *B. ceiba* wood dust using three different chemical activating agents – phosphoric acid, potassium hydroxide, and sodium carbonate – followed by carbonization at an optimized temperature determined through thermogravimetric (TG) analysis and differential scanning calorimetry. The optimal carbonization temperature was identified as 400°C. AC samples were prepared through a one-step chemical impregnation and carbonization process under nitrogen flow. Comprehensive characterization using X-ray diffraction, Raman spectroscopy, Fourier-transform infrared spectroscopy, scanning electron microscopy, and Brunauer–Emmett–Teller surface area analysis confirmed the formation of amorphous carbon structures with abundant oxygenated surface functional groups and porous architectures. Among the three samples, phosphoric acid-activated carbon (Bc-H) exhibited the highest surface area (1,451.2 m^2/g) and a well-developed micro–mesoporous structure. Batch adsorption experiments showed that Bc-H achieved 99.9% RhB removal under optimized conditions (20 ppm initial dye concentration, pH 8.5, 0.03 g adsorbent, 10 min). Its superior performance is attributed to its large surface area and rich surface functionalities. Notably, Bc-H also outperformed commercial AC under identical conditions, demonstrating faster kinetics and higher removal efficiency. These findings underscore *B. ceiba* wood dust as a low-cost and sustainable precursor for high-performance AC production. The work contributes to waste biomass valorization and offers a scalable, eco-friendly solution for industrial wastewater treatment, particularly relevant to textile and dyeing effluents in resource-limited settings such as Nepal.

Keywords: *Bombax ceiba*; Activated carbon; Rhodamine B adsorption; Wastewater treatment; Chemical activation; Sustainable adsorbent

1. Introduction

The growing demand for clean water, coupled with the intensification of industrial activities, has significantly increased the release of synthetic dyes into aquatic ecosystems. Among these, rhodamine B (RhB) – a xanthene-based cationic dye widely used in the textile, paper, plastic, and cosmetic industries[1] – has attracted serious concern due to its high water solubility, photostability, and toxic persistence.[2] RhB

is not only resistant to biodegradation but also exhibits carcinogenic and mutagenic properties, posing major environmental and public health risks.[3] Consequently, it is frequently employed as a model pollutant in adsorption studies for evaluating the efficiency of novel adsorbent materials in treating dye-contaminated industrial effluents. Adsorption is widely regarded as one of the most effective, economical, and environmentally friendly techniques for dye removal. Activated carbon (AC) remains the benchmark adsorbent due to its large surface area, well-developed porosity, and abundance of surface functionalities.[4] However, the commercial-scale use of AC is often constrained by high production costs and dependence on non-renewable precursors – limitations that are particularly challenging in resource-limited settings such as Nepal.

In Nepal, approximately 70% of industrial effluents – including those from textile and dyeing operations – are discharged untreated into rivers and streams, contributing to elevated concentrations of synthetic dyes in surface water bodies.[5] This growing dye pollution is further exacerbated by rapid industrialization, poor regulatory enforcement, and the lack of centralized wastewater treatment infrastructure. As a result, surface water quality continues to deteriorate, threatening aquatic ecosystems and public health. These challenges highlight the urgent need for low-cost, effective, and scalable dye remediation strategies, such as those explored in the present study.

To address these challenges, growing attention has been directed toward biomass-derived ACs, which offer a low-cost alternative while simultaneously valorizing agro-industrial and forestry residues. In this context, *Bombax ceiba* – commonly known as the silk cotton tree – has emerged as a promising lignocellulosic feedstock.[6] It is wood dust, a byproduct of the furniture and carpentry industries, widely available across Nepal, yet remains underutilized or discarded. Despite its abundance, only a few studies have explored the potential of *B. ceiba* wood dust for AC production, and none have systematically investigated the influence of different chemical activating agents on its dye adsorption performance.[7] This gap forms the basis and core novelty of the present work. The novelty of this study lies in its first-ever systematic comparison of acid (phosphoric acid [H_3PO4]), base (potassium hydroxide [KOH]), and salt (sodium carbonate [Na_2CO3]) activation routes applied to *B. ceiba* wood dust for the development of high-performance AC adsorbents. This approach is unique in evaluating how different chemical activating agents influence the structure, surface chemistry, and RhB dye adsorption efficiency of carbons derived from the same biomass.

In addition, the study integrates thermogravimetric analysis (TGA)/differential scanning calorimetry (DSC)-based thermal optimization and demonstrates ultrafast RhB removal with high efficiency, outperforming commercial AC. A carbonization temperature of 400°C was selected based on TGA/DSC analysis, which indicated significant thermal decomposition and stabilization of the biomass structure around this temperature. This activation strategy represents a key innovation of the study, enabling a direct comparison of acid-, base-, and salt-mediated activation routes on the same biomass – an approach rarely reported in the literature.[8] These findings provide both mechanistic insight and practical value for developing cost-effective, sustainable adsorbents for wastewater remediation, particularly in resource-limited settings like Nepal.

The resulting ACs – H_3PO_4-activated carbon (Bc-H), KOH-activated carbon (Bc-K), and Na_2CO_3-activated carbon (Bc-Na) – were comprehensively characterized using X-ray diffraction (XRD), Raman spectroscopy, Fourier-transform infrared spectroscopy (FTIR), scanning electron microscopy (SEM), and Brunauer–Emmett–Teller (BET) surface area analysis to evaluate their structural, morphological, and surface chemical properties. Their RhB adsorption performance was subsequently assessed under varying operational parameters, including dye concentration, solution pH, adsorbent dosage, and contact time.[9] Among these, Bc-H exhibited the highest performance, achieving a surface area of 1,451.2 m^2/g and a maximum RhB removal efficiency of 99.9% under optimized conditions. This superior behavior is attributed to its extensive surface area, highly developed pore structure, and the abundance of oxygenated surface groups.

Overall, this study presents a waste-to-resource approach strategy for *B. ceiba* wood dust and offers a comparative framework for optimizing chemical activation routes. The resulting material served as a cost-effective and efficient adsorbent for RhB removal, with particular relevance to the textile and dyeing sectors.[10] The findings contribute to the development of sustainable and scalable wastewater treatment technologies, offering practical solutions for regions seeking affordable, environmentally friendly alternatives aligned with global sustainability goals.

2. Materials and methods

2.1. Materials and reagents

All chemicals used in this study were of analytical reagent grade and employed without further purification. H_3PO_4 (85%) was obtained from Fisher Scientific (India), while potassium KOH (pellets) and Na_2CO_3 (anhydrous) were procured from Merck (Merck Specialties Pvt. Ltd., India). These three chemicals served as activating agents for the synthesis of biomass-derived AC.

RhB (≥98%), used as the model dye pollutant, was purchased from Alfa Aesar (product code: A13572; Haverhill, USA). Aqueous ammonia (30%) from Baker (J.T. Baker, USA) was used to adjust the solution pH during adsorption studies. All aqueous solutions were prepared using double-distilled water to minimize interference from residual ions or impurities.

The raw biomass precursor, *B. ceiba* wood dust (locally known as "Simal" in Nepal), was collected as waste from a sawmill in Kathmandu, Nepal. This lignocellulosic byproduct, selected for its abundance and underutilization, was first washed thoroughly with distilled water to remove surface contaminants, then sun-dried and sieved to achieve a uniform particle size suitable for activation and carbonization.

2.2. Preparation of ACs

2.2.1. Pre-treatment of biomass

The *B. ceiba* wood dust was first washed with distilled water to remove surface dust, debris, and water-soluble impurities. The cleaned material was then sun-dried for 2 – 3 days and subsequently oven-dried at 110°C for 24 h to eliminate residual moisture and volatiles. After drying, the biomass was finely ground and sieved through a 150 μm mesh to obtain a uniform particle size, ensuring consistency during chemical activation and carbonization.

The impregnation ratio of biomass to activating agent was fixed at 1:1, based on prior optimization trials in which ratios such as 1:2, 2:1, 1:0.5, and 0.5:1 were evaluated. Among these, the 1:1 ratio consistently yielded the most favorable balance between surface area development and RhB adsorption efficiency across different activating agents.

2.2.2. Thermogravimetric (TG) and DSC analysis for carbonization optimization

To determine the optimal carbonization temperature, TGA coupled with DSC was performed on raw *B. ceiba* wood powder. The thermal degradation profile revealed significant mass loss between 200°C and 400°C, corresponding to the decomposition of hemicellulose, cellulose, and partially degraded lignin components.[1,11] Based on this thermal behavior, 400°C was selected as the carbonization temperature, offering a favorable compromise between carbon yield, thermal stability, and porosity development for effective activation.

2.2.3. Chemical activation and carbonization

ACs were prepared using three different chemical activating agents – an acid (H_3PO_4), a base (KOH), and a salt (Na_2CO_3) – to produce samples designated as Bc-H, Bc-K, and Bc-Na, respectively. A 1:1 weight ratio of dried *B. ceiba* wood powder to the activating agent was maintained. The biomass was impregnated by soaking in the respective chemical solution for approximately 12 h to allow thorough interaction, after which the samples were subsequently oven-dried at 110°C to remove residual moisture.

The dried, impregnated material was then subjected to carbonization in a horizontal tubular furnace at the optimized temperature of 400°C (as determined by TGA/DSC), with a heating rate of 10°C/min. The final temperature was maintained for 3 h under a continuous flow of nitrogen gas (100 mL/min) to ensure an inert atmosphere throughout the process.

This one-step chemical activation and carbonization method facilitated the formation of porous carbon structures with distinct physicochemical properties, largely influenced by the type of activating agent used.[2,12]

2.2.4. Post-treatment

Following carbonization, the resulting black solids were allowed to cool naturally under a continuous nitrogen flow. Each sample – Bc-H, Bc-K, and Bc-Na – was thoroughly washed with double-distilled water until the filtrate reached neutral pH (~7.0), ensuring the removal of residual activating agents and soluble byproducts. The cleaned materials were then oven-dried at 110°C, finely ground into a fine powder, and stored in airtight containers for subsequent characterization and adsorption experiments. Table 1 summarizes the preparation parameters for the chemically AC samples synthesized from *B. ceiba* wood dust.

2.3. Adsorption experiments

Batch adsorption experiments were conducted to evaluate the efficiency of AC samples – Bc-H, Bc-K, and Bc-Na – in removing RhB from aqueous solutions. A 20 ppm stock solution of RhB was prepared by dissolving 20 mg of the dye in 1 L of double-distilled

Table 1. Summary of preparation parameters for chemically activated carbons

Parameter	Condition
Biomass precursor	*Bombax ceiba* (Simal) wood dust
Particle size	100 µm
Activating agents	Phosphoric acid (Bc-H), potassium hydroxide (Bc-K), and sodium carbonate (Bc-Na)
Impregnation ratio	1:1 (w/w)
Impregnation time	Overnight (~12 h)
Pre-drying temperature	110°C
Carbonization temperature	400°C
Carbonization duration	Three hours
Atmosphere	Nitrogen gas (inert)
Final drying	110°C

water. To optimize experimental parameters, preliminary tests were carried out at varying initial dye concentrations (above and below 20 ppm) and at pH values of 3.5, 6.5, 8.5, and 10.5. Based on these trials, 20 ppm dye concentration and pH 8.5 were found to yield the highest removal efficiency and were selected for subsequent kinetic and comparative studies.

For each batch adsorption test, 100 mL of the dye solution was transferred to a 250 mL Erlenmeyer flask, followed by the addition of 0.02 g of AC. The mixture was stirred at 400 rpm for 10 min using a magnetic stirrer, under ambient conditions, at the optimized pH. During adsorption, 3 mL aliquots were withdrawn at 2-min intervals (0, 2, 4, 6, 8, and 10 min), transferred to microcentrifuge tubes, and centrifuged for 5 min to separate the carbon particles. The supernatants were analyzed using an ultraviolet-Vis spectrophotometer (SCINCO Mega-2100, double beam, SCINCO, South Korea) to measure the residual RhB concentration.

To investigate the effect of adsorbent dosage, the experiment was repeated using different carbon masses (0.02 g, 0.025 g, 0.03 g, and 0.035 g). The influence of solution pH on adsorption efficiency was also assessed by conducting tests at the same pH values used in the preliminary trials. The percentage of dye removed was calculated using the following formula in Equation I:

$$\% \text{ Removal} = (Co - Ce)/Co \times 100\% \quad (I)$$

where Co is the initial dye concentration (mg/L), and Ce is the equilibrium dye concentration after adsorption (mg/L).

This systematic approach enabled the optimization of adsorption parameters and provided a comparative evaluation of the dye removal performance of the ACs synthesized with different chemical agents.

2.4. Characterization techniques of AC samples

Comprehensive physicochemical characterization was conducted to evaluate their thermal behavior, morphology, crystallinity, functional groups, structural disorder, and surface textural properties of the raw biomass and synthesized AC samples, all of which are critical for understanding their adsorption performance.

2.4.1. Thermal analysis

TGA and DSC were performed using an SDT Q600 V20.9 Build 20 system (TA Instruments, USA) to analyze the pyrolytic behavior of sieved wood powder of (raw) *B. ceiba* wood dust and to determine the optimal carbonization temperature.

2.4.2. Morphological characterization

The surface morphology and porosity of the AC samples were examined using SEM (Nanoeyes SEM, South Korea) to observe surface texture, pore development, and particle structure.

2.4.3. Phase analysis

The structural order of the carbon samples was assessed through XRD using a Rigaku RINT 2000 Diffractometer (Rigaku Corporation, Japan). Broad diffraction peaks were analyzed to distinguish amorphous features and crystalline tendencies.

2.4.4. Functional group identification

Fourier transform infrared spectroscopy was carried out using a Bruker Vertex 70 (Bruker, Germany) to identify surface functional groups. Spectra were recorded in the 4,000 – 400 cm^{-1} range with a resolution of 4 cm^{-1}, highlighting oxygenated functionalities such as hydroxyl, carboxyl, phosphate, and ether groups.

2.4.5. Structural disorder evaluation

Raman spectroscopy (LabRAM HR800, Jobin Yvon, Jobin Yvon, France), with a 532 nm excitation laser, was used to evaluate structural disorganization in the carbon samples. The intensity ratio of the D and G bands was used to quantify graphitic defects and amorphous content.

2.4.6. Textural properties

The BET method was employed using a Micromeritics ASAP 2020 system (Micromeritics Instrument

Corporation, USA) after degassing the samples at 300°C for 6 h under vacuum to determine specific surface area, pore volume, and average pore diameter. These parameters were used to assess the adsorption potential of each sample.

2.4.7. Adsorption evaluation

Adsorption performance was evaluated using ultraviolet-Vis spectrophotometry (SCINCO Mega-2100, double beam at 554 nm with a 1 cm quartz cuvette; SCINCO Co., Ltd., South Korea) by monitoring RhB concentration changes during batch experiments. Absorbance data were used to calculate dye removal percentages under various conditions.

3. Results and discussion

3.1. Thermal degradation of *B. ceiba* wood powder

TGA and DSC were performed on raw B. ceiba wood powder to investigate its thermal decomposition profile and determine the optimal carbonization temperature. The TGA curve (red) illustrates the percentage mass loss, while the DSC curve (green) shows the corresponding heat flow during heating (Figure 1).

TG/DSC analysis results revealed a multistage degradation process typical of lignocellulosic biomass. Distinct mass loss events, accompanied by thermal transitions in the DSC curve, correspond to the decomposition of moisture, hemicellulose, cellulose, and lignin components.[11,13]

(i) Initial mass loss (room temperature to ~150°C): A minor weight reduction (~8 – 10%) occurred up to 150 °C due to the evaporation of physically adsorbed water. This is associated with a mild endothermic dip in the DSC curve, reflecting energy absorption during moisture loss.

(ii) Active pyrolysis phase (~200 – 400°C): The major decomposition phase occurred between 200°C and 400°C, accounting for a ~60% mass loss. This corresponds to the breakdown of hemicellulose (200 – 300°C) and cellulose (300 – 400°C).[11] The strong exothermic peak in the DSC curve indicates significant heat release during pyrolytic degradation and volatile matter evolution.

(iii) Optimal carbonization zone (~400°C): Around 400°C, a sharp decline in the TGA curve and an intense exothermic peak in the DSC profile signaled the completion of cellulose degradation and the onset of lignin breakdown.[10] This temperature marks the transition from volatile release to the formation of a carbon-rich matrix. Therefore, 400°C was selected as the carbonization temperature, offering a balance between carbon yield and structural stability.

(iv) Residual mass stabilization (above 400°C): Beyond 400°C, the rate of mass loss decreased significantly, indicating the slow degradation of lignin and the stabilization of char. The remaining mass (~20%) reflects a thermally stable carbonaceous structure, while the extended exothermic tail suggests ongoing reorganization of carbon domains.

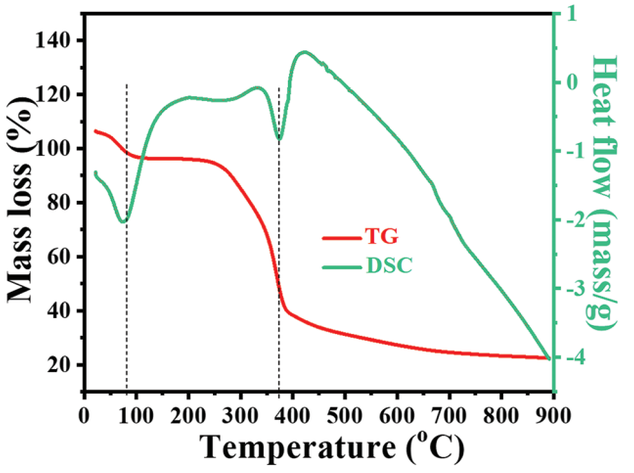

Figure 1. Thermogravimetric (TG)/differential scanning calorimetry (DSC) analysis of raw *Bombax ceiba* wood powder

The TG/DSC analysis confirms a typical multi-phase thermal degradation of lignocellulose, with moisture loss, followed by hemicellulose and cellulose decomposition, and gradual lignin breakdown. The thermal behavior indicates that 400°C is an appropriate carbonization temperature for *B. ceiba* biomass, enabling effective removal of volatiles and stabilization of the carbon framework.[14] This optimized temperature was adopted for preparing ACs with favorable porosity and structural integrity for adsorption and environmental applications.

3.2. Material characterization of prepared ACs

3.2.1. XRD analysis

The XRD analysis was performed to assess the crystallinity and structural order of AC samples synthesized from *B. ceiba* wood dust using different chemical activating agents. The XRD patterns of Bc-H, Bc-K, and Bc-Na are presented in Figure 2.

All three samples exhibited a broad diffraction peak centered around 2θ ≈ 26 – 27°, corresponding to the (002) plane of graphitic carbon. This feature is

characteristic of turbostratic or disordered carbon, where carbon atoms exhibit short-range order but lack the long-range periodicity found in crystalline graphite. The broadness and low intensity of the (002) peak reflect a predominantly amorphous structure, which is common in chemically-ACs produced at moderate temperatures (~400°C).[15]

In addition, a weaker, broader peak was sometimes observed near 2θ ≈ 43°, corresponding to the (100) or (101) planes. However, in these samples, it is either absent or poorly resolved, reinforcing the low degree of crystallinity and suggesting irregular layer stacking and structural disorder in the carbon matrix.

The absence of sharp crystalline peaks from activating agents (e.g., potassium chloride, sodium chloride, or phosphate salts) indicates the effective removal of residual inorganic compounds during the post-carbonization washing process. This confirms successful chemical activation and purification steps in producing clean, functional carbon materials.[16]

Bc-H exhibited a relatively broader and more diffuse (002) peak, consistent with highly amorphous carbon and well-developed porosity. H_3PO_4 acts as a crosslinking and dehydrating agent, facilitating polyphosphoric network formation and preventing excessive structural ordering during carbonization.

Bc-K showed a slightly sharper (002) peak than Bc-H, possibly due to the formation of localized microcrystalline domains or graphitic clusters, although still largely amorphous. KOH activation is known to etch the carbon framework and promote microporosity, but complete graphitization typically requires higher temperatures (>700°C).

Bc-Na displayed the weakest and broadest (002) reflection, indicating the least graphitic characteristic and highest disorder among the three. This suggests that Na_2CO_3 is less effective at enhancing structural order under the studied conditions.

Overall, the XRD results confirm that all samples are predominantly amorphous with turbostratic carbon domains, suitable for adsorption applications due to their high defect density and surface activity. The differences in peak sharpness and position reflect the impact of the activation agent on carbon structure evolution, with Bc-H exhibiting the most disordered but functionally favorable structure for dye adsorption.

3.2.2. Raman spectroscopy

Raman spectroscopy was employed to further assess the degree of structural order and graphitic characteristics in the AC samples derived from *B. ceiba* wood dust. Figure 3 presents the Raman spectra of Bc-H, Bc-K, and Bc-Na.

All samples exhibited the two characteristic bands of carbonaceous materials. The D band (~1,351 cm^{-1}) is associated with lattice defects, sp^3-hybridized carbon, and disordered domains, while the G band (~1,597 cm^{-1}) is attributed to the E_2g vibrational mode of sp^2-hybridized carbon atoms in graphitic planes.[17]

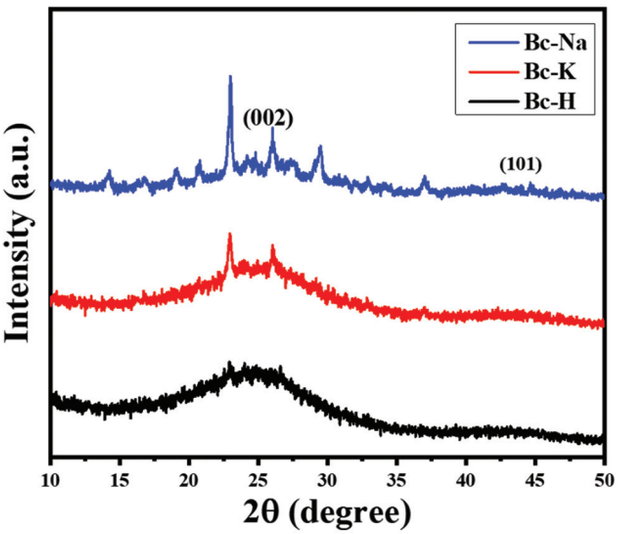

Figure 2. X-ray diffraction patterns of chemically activated carbon (AC) samples. Bc-H, Bc-K, and Bc-Na refer to acid-activated, base-activated, and salt-ACs, respectively.

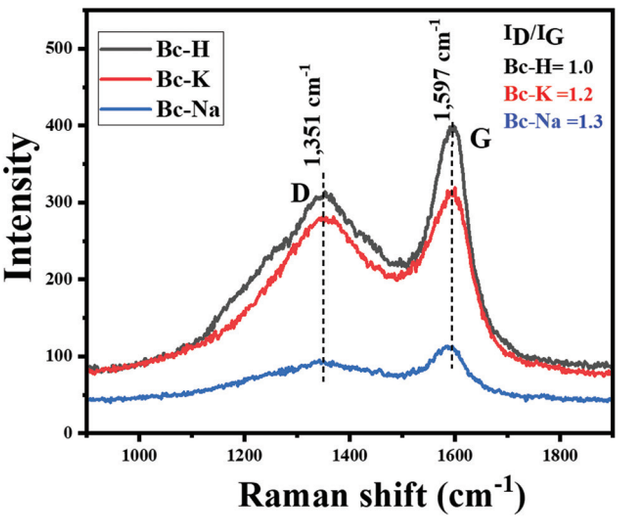

Figure 3. Raman spectra of chemically activated carbon (AC) samples. Bc-H, Bc-K, and Bc-Na refer to acid-activated, base-activated, and salt-ACs, respectively. ID/IG refers to the intensity ratio of the D bands to the G bands.

The intensity ratio of the D to G bands (ID/IG) serves as a semi-quantitative indicator of disorder. The calculated ID/IG values were 1.0, 1.2, and 1.3 for Bc-H, Bc-K, and Bc-Na, respectively. These results indicate that Bc-H possessed the lowest degree of structural disorder, suggesting a relatively more ordered sp^2 carbon network compared to Bc-K[17] and Bc-Na. This observation correlates well with the XRD results, which also revealed a somewhat better-defined (002) peak for Bc-H, although the structure still remains largely disordered and turbostratic (amorphous).

When interpreting the structure of the ACs, Bc-H exhibited moderate graphitization and fewer defects, which may enhance uniformity in surface chemistry and facilitate better adsorption. Bc-K and Bc-Na had higher ID/IG ratios, reflecting more disordered structures and greater defect densities, which are consistent with the broader Raman and XRD features.

All samples are predominantly amorphous, as confirmed by XRD and Raman analyses. However, Bc-H displayed comparatively lower disorder and a more organized carbon matrix. This improved structural integrity may support more efficient dye adsorption and contribute to enhanced performance in environmental or electrochemical applications.[18]

3.2.3. SEM analysis

The surface morphologies of the AC samples – Bc-H, Bc-K, and Bc-Na – were examined through SEM, as presented in Figure 4. The results illustrate how chemical activation and thermal treatment influence pore formation and surface texture in the *B. ceiba*-derived carbons.

All samples exhibited porous features formed through activating agent-driven etching of the biomass during carbonization.[18] These chemical activators promote porosity by reacting with the carbon matrix, causing dehydration, expansion, and localized leaching.[19]

Bc-H displayed a fragmented and highly porous morphology, with interconnected mesopores clearly visible. This structure reflects the dual role of H_3PO_4 as both a dehydrating and crosslinking agent. During carbonization, H_3PO_4 stabilizes the carbon framework and inhibits tar formation, resulting in uniform pore development and enhanced structural integrity. The well-formed mesoporous network observed in Bc-H corresponds closely with its high BET surface area and amorphous characteristics, as supported by XRD and Raman data. Notably, prior studies have shown that H_3PO_4 activation is effective at moderate temperatures (400 – 500°C),[20] consistent with the pore development observed in this study.

The Bc-K sample exhibited a more compact and layered surface with fewer discernible pores. While KOH is a well-established activating agent, it generally requires higher temperatures (700 – 800°C) to promote effective microporosity through redox interactions with carbon.[21] At 400°C, these reactions are limited, leading to underdeveloped pore structures and low mesoporosity. The SEM findings align with Bc-K's relatively low surface area and higher disorder, as revealed by BET and Raman analyses, indicating incomplete activation at the applied temperature.

The Bc-Na sample revealed a porous yet irregular morphology, featuring macro pore-like voids and signs of localized expansion macro pore-like voids and signs of localized expansion. These features are likely caused by internal gas release and thermal stress during Na_2CO_3 decomposition. However, similar to KOH, effective activation with Na_2CO_3 typically requires higher temperatures (~700°C or above) for sufficient pore development.[13,21] The 400°C treatment used here likely limited its activating effect, resulting in uneven porosity and reduced mesopore content.

SEM analysis revealed clear differences in pore morphology among the AC samples. Bc-H showed the

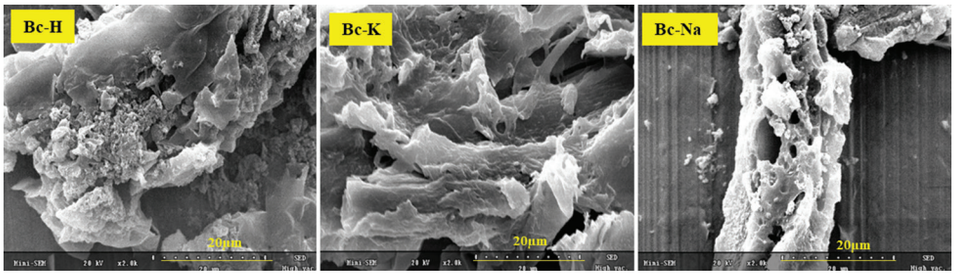

Figure 4. Scanning electron microscopic images of Bc-H, Bc-K, and Bc-Na samples. Bc-H, Bc-K, and Bc-Na refer to acid-activated, base-activated, and salt-activated carbons, respectively. Scale bar: 20 µm, magnification: 20,000×.

most developed and uniform mesoporous structure, attributed to the efficient activating effect of H_3PO_4 at 400°C. In contrast, Bc-K and Bc-Na exhibited suboptimal activation, with denser or irregular surfaces due to insufficient thermal conditions for their respective activating chemistries. These morphological trends are consistent with BET surface areas and structural disorder observed through Raman and XRD, reinforcing the superior activation achieved in Bc-H.

While SEM revealed the general surface morphology, higher-resolution imaging (e.g., transmission electron microscopy) could further elucidate nanostructural features and will be considered in future studies.

3.2.4. Nitrogen adsorption/desorption isotherm and BET surface area analysis

Nitrogen adsorption/desorption isotherms at 77 K were recorded for Bc-H, Bc-K, and Bc-Na to evaluate their surface area and pore characteristics (Figure 5).

All three samples exhibited a sharp increase in nitrogen uptake at low relative pressure ($P/P_0 < 0.1$), indicative of microporous structures. Among them, Bc-H showed the most pronounced uptake, suggesting a higher micropore volume than Bc-K and Bc-Na.

At higher relative pressures ($P/P_0 = 0.5 – 1.0$), Bc-H displayed a distinct hysteresis loop, characteristic of mesopore-induced capillary condensation. This behavior reflects a well-developed mesoporous network, which correlates with the highly porous surface observed in SEM images. In contrast, Bc-K and Bc-Na showed minimal or no hysteresis, implying more limited mesoporosity and a predominance of micropores.

Quantitative textural parameters – BET surface area, average pore size, and total pore volume – are summarized in Table 2. Bc-H possesses a BET surface area of 1,451.2 m^2/g, average pore size of 5.5 nm, and a total pore volume of 1.8 cm^3/g, demonstrating a highly porous architecture. These attributes can be attributed to the effective action of H_3PO_4, which promotes dehydration and crosslinking during activation, facilitating the development of both micro- and mesopores.[22]

In comparison, Bc-K and Bc-Na exhibited much lower surface areas (78.4 m^2/g and 61.2 m^2/g, respectively). Their narrower pore size distributions and weaker mesoporosity are largely due to the suboptimal activation temperature (400°C), which is insufficient for effective activation by KOH and Na_2CO_3. Both of these agents typically require temperatures above 700 – 800°C for full activation and porosity development.

Overall, the BET and isotherm results further confirm that Bc-H has superior surface textural properties, which are expected to significantly enhance its adsorption efficiency and applicability in energy storage systems.

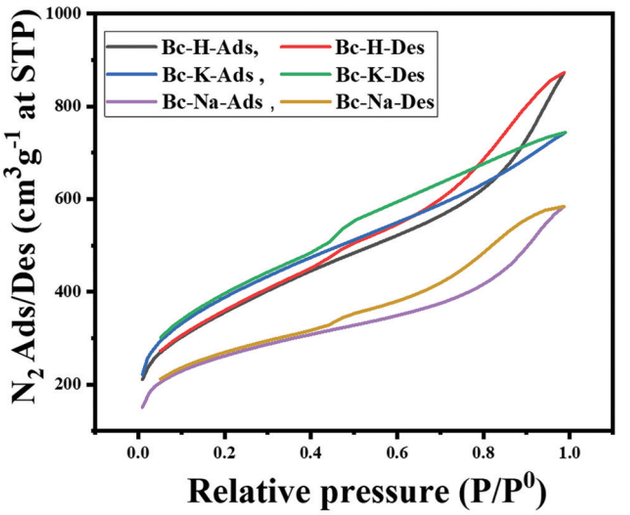

Figure 5. Nitrogen (N_2) adsorption (Ads)/desorption (Des) isotherms of Bc-H, Bc-K, and Bc-Na measured at 77 K (standard temperature [STP] for N_2 Ads experiments). Bc-H, Bc-K, and Bc-Na refer to acid-activated, base-activated, and salt-activated carbons, respectively.

Table 2. Brunauer–Emmett–Teller surface area, average pore size, and total pore volume of samples

Sample	Brunauer–Emmett–Teller surface area (m^2/g)	Average pore size (nm)	Total pore volume (cm^3/g)
Bc-H	1451.2	5.5	1.8
Bc-K	78.4	3.5	0.25
Bc-Na	61.2	4.2	0.15

Note: Bc-H, Bc-K, and Bc-Na refer to acid-activated, base-activated, and salt-activated carbons, respectively.

3.2.5. FTIR analysis

The FTIR spectra of the AC samples (Bc-H, Bc-K, and Bc-Na), recorded in the range of 4,000 – 400 cm^{-1}, are shown in Figure 6. This analysis highlights the influence of different chemical activating agents on the surface functional groups of the carbons.

A broad absorption band around 3,335 – 3,420 cm^{-1}, most prominent in Bc-Na and Bc-H, corresponds to the hydroxyl (–OH) group stretching vibrations, indicating the presence of hydroxyl groups from alcohols, phenolic groups, as well as adsorbed moisture. The relatively reduced intensity of this band in Bc-K suggests more

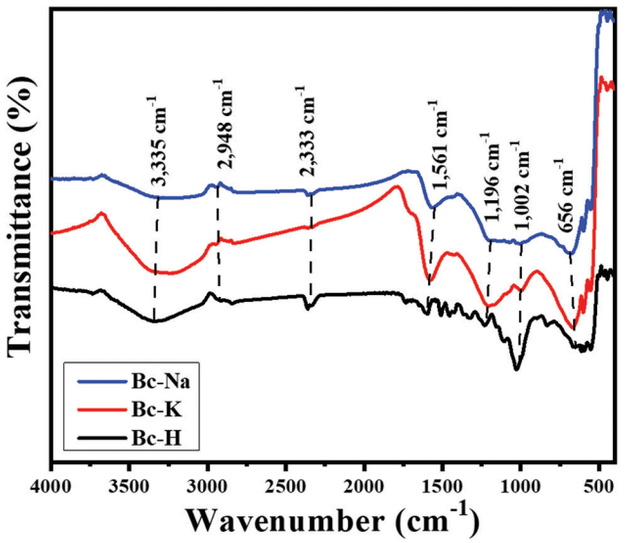

Figure 6. Fourier-transform infrared spectroscopy spectra of chemically activated carbon (AC) samples. Bc-H, Bc-K, and Bc-Na, showing characteristic peaks of surface functional groups after activation. Bc-H, Bc-K, and Bc-Na refer to acid-activated, base-activated, and salt-ACs, respectively.

effective dehydration during KOH activation, in agreement with TGA/DSC results.[13]

A weak band near 2,948 cm^{-1} across all samples is attributed to aliphatic C–H stretching, while a minor feature at 2,333 cm^{-1} may arise from atmospheric carbon dioxide or asymmetric stretching of methyl groups.

The band observed near 1,561 – 1,600 cm^{-1} is assigned to C=C stretching in aromatic rings, indicating the development of conjugated graphitic domains.[18] This feature is more intense in Bc-K and Bc-Na, suggesting a higher degree of carbonization under alkaline activation.

In the region between 1,200 and 1,000 cm^{-1}, multiple peaks are present. Bands at 1,196 cm^{-1} and 1,002 cm^{-1} correspond to C–O stretching in alcohols, esters, and carboxylic acids. A strong band around 1,240 cm^{-1} in Bc-H is attributed to P=O stretching, while features near 1,040 – 1,100 cm^{-1} are associated with P–OH and ether (C–O–C) linkages, which are introduced during H_3PO_4 activation. A small peak at 656 cm^{-1} is attributed to C–H bending or out-of-plane deformation of substituted aromatics.

Overall, Bc-H retained a higher abundance of O–H, C–O, and P-containing surface groups due to the milder dehydrating and crosslinking action of H_3PO_4, which preserves polar functionalities. In contrast, Bc-K and Bc-Na exhibited sharper C=C bands and fewer polar groups, consistent with higher thermal degradation and deoxygenation during alkaline activation.[14] These surface functionalities are crucial for dye adsorption. In particular, hydroxyl, carbonyl, phosphate, and aromatic groups are expected to facilitate electrostatic attraction, hydrogen bonding, and π–π stacking interactions with Rh B molecules, enhancing adsorption capacity and rate.

3.2.6. Physicochemical properties in the adsorption of cationic dye

The adsorption performance of the AC samples toward RhB is strongly influenced by their physicochemical characteristics, as revealed by XRD, Raman spectroscopy, SEM, BET, and FTIR analyses.

The XRD patterns and Raman spectra confirm the predominantly amorphous nature of the samples, with broad diffraction peaks and a high D/G band intensity ratio. This structural disorder increases defect sites on the carbon matrix, which serve as active centers for π–π stacking interactions with the aromatic structure of RhB.

The SEM micrographs illustrate highly porous irregular surface morphologies – particularly for Bc-H – that enhance external surface accessibility and facilitate dye molecule penetration. These observations are consistent with BET analysis, which showed substantial surface area and mesoporosity, both essential for rapid adsorption kinetics and high capacity.

The FTIR spectra further reveal the presence of oxygen-containing functional groups such as hydroxyl, carboxylic, and carbonyl moieties. These functionalities promote electrostatic interactions and hydrogen bonding with the cationic RhB molecules, increasing adsorption affinity. Taken together, the synergistic combination of amorphous carbon structure, high defect density, hierarchical porosity, and rich surface functionality underpins the strong dye adsorption capacity of the synthesized carbons. These integrated properties highlight their potential for efficient RhB removal in wastewater treatment applications.

3.3. Adsorption studies

The adsorption performance of the synthesized AC samples – Bc-H, Bc-K, and Bc-Na – was systematically evaluated for RhB removal under various experimental conditions. Key parameters such as solution pH, adsorbent dosage, and contact time were optimized to assess adsorption kinetics and efficiency.

3.3.1. Comparative performance of chemically-ACs and commercially-AC

Before analyzing parameter-specific adsorption trends, a baseline performance of the three synthesized carbons under fixed conditions (20 ppm RhB, pH 8.5, 0.03 g adsorbent) was determined. The ultraviolet-Vis absorption spectra presented in Figure 7 illustrate the variation in dye removal among Bc-H, Bc-K, and Bc-Na.

Among the three, Bc-H exhibited rapid and nearly complete RhB removal within 2 – 4 min, as confirmed by the significant reduction in the absorbance peak at ~554 nm. This superior performance can be attributed to its favorable physicochemical characteristics: an amorphous carbon structure with high defect density, well-developed mesoporosity, large surface area, and abundant oxygen-containing surface functional groups (–OH, carboxyl [–COOH], and carbonyl [–C=O]). These properties collectively enhance π–π stacking, electrostatic attraction, hydrogen bonding, and dye diffusion.

In contrast, Bc-K demonstrated limited adsorption, with partial dye removal observed even after 10 min. Bc-Na showed negligible adsorption, likely due to its low surface area, limited porosity, and insufficient functional group density. These results are consistent with the SEM, BET, and FTIR analyses.

To benchmark these findings, the performance of Bc-H was compared against commercial AC under identical conditions. As shown in Figure 8, Bc-H achieved faster and more complete dye removal than the commercial AC, which exhibited slower kinetics and incomplete RhB adsorption even after 10 min.

These comparative results affirm that Bc-H not only outperformed the other lab-synthesized carbons but also exceeded the performance of commercial AC, making it a strong candidate for practical wastewater treatment applications.

Based on these outcomes, subsequent detailed adsorption studies – focusing on pH, dosage, and contact time – were carried out exclusively for Bc-H. This selection is justified by its consistently superior performance across all experimental parameters.

3.3.2. Effect of variable parameters

(a) Effect of pH on RhB adsorption by phosphoric acid-AC

A solution's pH plays a critical role in adsorption by influencing the surface charge of the adsorbent, the ionization state of the adsorbate, and the interactions between them. To determine the optimal pH for RhB adsorption by Bc-H, experiments were conducted at four initial pH levels: 3.5, 6.5, 8.5, and 10.5. A constant adsorbent dose of 0.03 g was used based on preliminary trials across various dosages (0.02 – 0.035 g). Results are presented in Figure 9.

At pH 8.5, Bc-H achieved near-complete removal of RhB within 6 – 10 min, as evidenced by the disappearance of the absorption peak near 550 nm. In contrast, adsorption at pH 3.5 and 10.5 was significantly less efficient. RhB absorption at pH 6.5 showed moderate improvement but did not achieve complete removal within the same time frame.

The influence of pH on adsorption can be attributed to two main factors: RhB speciation and the surface charge of Bc-H. RhB is a xanthene-based dye that predominantly exists in a cationic form in aqueous solution across a wide pH range. However, its molecular structure and charge distribution can undergo subtle changes depending on the pH,

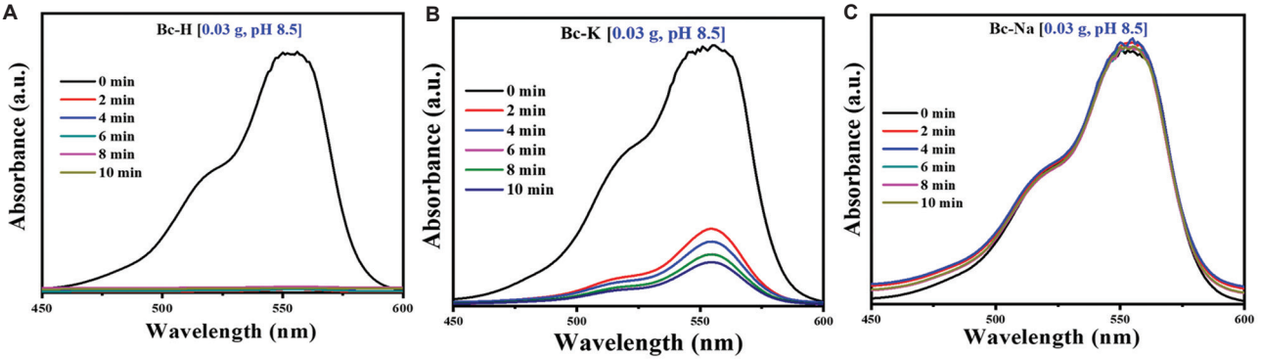

Figure 7. Comparative ultraviolet-Vis absorption spectra of RhB solutions after treatment with (A) Bc-H, (B) Bc-K, and (C) Bc-Na at different contact times (0 – 10 min) under identical conditions (0.03 g adsorbent, pH 8.5). Bc-H, Bc-K, and Bc-Na refer to acid-activated, base-activated, and salt-ACs, respectively.

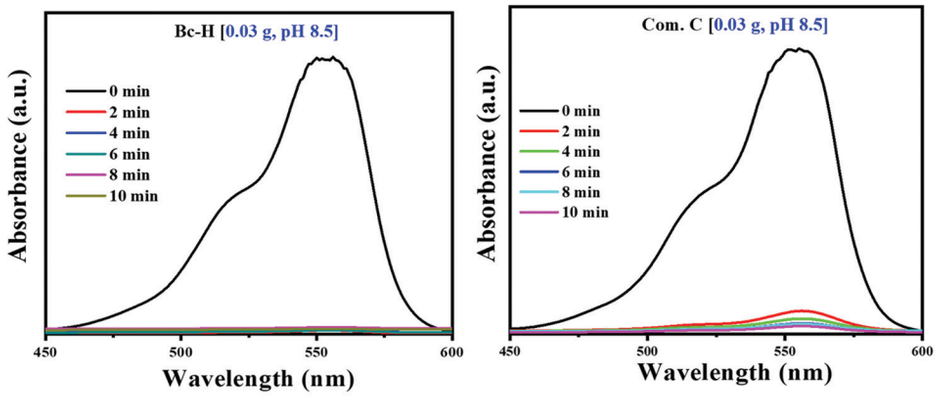

Figure 8. Comparison of rhodamine B adsorption performance between phosphoric acid-activated carbon (Bc-H) and commercially-activated carbon at 0.03 g adsorbent dose and pH 8.5 over different contact times

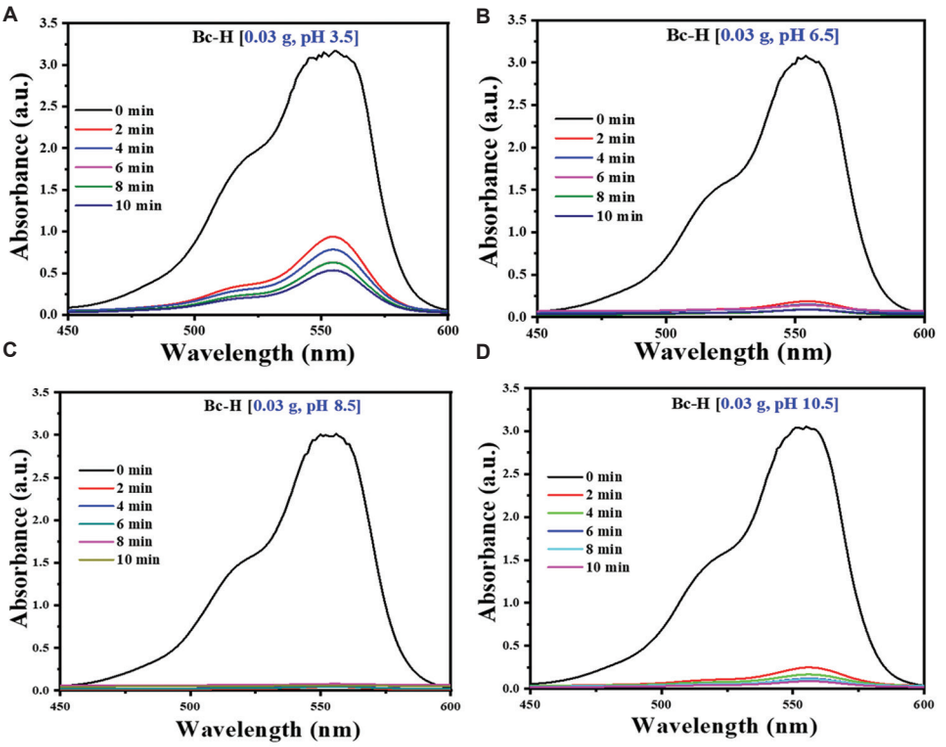

Figure 9. Ultraviolet-vis spectra showing rhodamine B adsorption by phosphoric acid-activated carbon (Bc-H) at different pH values. (A) pH 3.5, (B) pH 6.5, (C) pH 8.5, (D) pH 10.5

which in turn influences its adsorption behavior. At low pH (acidic conditions), RhB exists mainly as a fully protonated cation, with the amino group in its $–NR_2H^+$ form. The dye remains highly soluble, and electrostatic interactions are primarily governed by its overall positive charge. At neutral to mildly alkaline pH, the molecule remains cationic, but its structure becomes more stabilized for adsorption due to minimal repulsion with the negatively charged adsorbent surface (as in Bc-H). This condition typically favors strong electrostatic attraction and π–π stacking with the carbon surface. At elevated to high pH (≥9), RhB may undergo partial deprotonation of the –COOH group, resulting in the formation of a zwitterionic species. This species carries both a positively charged $–NR_2H^+$ group and a negatively charged $–COO^–$ group, coexisting within the same molecule.[15] Although the zwitterionic form is not dominant, it increases the dipole moment of the molecule, potentially altering

adsorption orientation, mobility, and affinity toward charged surfaces. In addition, changes in polarity may influence the extent of self-aggregation in solution.

At very high pH (above 10), aggregation, micelle-like behavior, or partial precipitation may occur due to reduced solubility, which lowers the concentration of freely available dye molecules for adsorption.[16] Excess hydroxide ions (OH^-) may also compete with RhB for active adsorption sites on the adsorbent surface.

In terms of surface charges, the surface charge of Bc-H is primarily governed by the protonation and deprotonation of its surface functional groups, particularly –OH, –COOH, and –C=O, introduced during H_3PO_4 activation.[23] The net surface charge varies with pH, directly influencing electrostatic interactions between the adsorbent and the cationic RhB molecules.

At low pH (e.g., pH 3.5), the acidic environment leads to protonation of surface functional groups, resulting in a positively charged surface. This condition induces electrostatic repulsion between Bc-H and the positively charged RhB molecules. In addition, excess hydrogen ions in the solution compete with dye molecules for active adsorption sites, further hindering adsorption efficiency. At near-neutral to mildly alkaline pH (6.5 – 8.5), progressive deprotonation of acidic surface groups occurs, rendering the Bc-H surface increasingly negatively charged. This enhances electrostatic attraction with cationic RhB molecules, thereby facilitating efficient adsorption.[24] The most favorable condition was observed at pH 8.5, where the balance between surface charge, dye solubility, and adsorbent integrity resulted in near-complete dye removal.

At high pH (e.g., pH 10.5), the adsorption efficiency declines despite the surface remaining negatively charged. This can be attributed to several factors: (i) dye aggregation or partial precipitation, reducing the number of free dye molecules available for adsorption, (ii) excess OH^- competing with RhB for active adsorption sites, and (iii) possible structural alteration or destabilization of surface functional groups under highly alkaline conditions, which may impair the binding capacity of Bc-H.[25] The percentage removal of RhB at each pH level is summarized in Figure 10.

Bc-H demonstrated the highest RhB adsorption efficiency at pH 8.5, attributed to strong electrostatic attraction and optimal surface conditions. At low pH, electrostatic repulsion and competition with protons inhibit adsorption; protonation of both adsorbent and dye leads to repulsion, while at high pH, aggregation and OH^- competition inhibit adsorption. These findings highlight the importance of pH optimization for maximizing dye removal using biomass-derived AC.

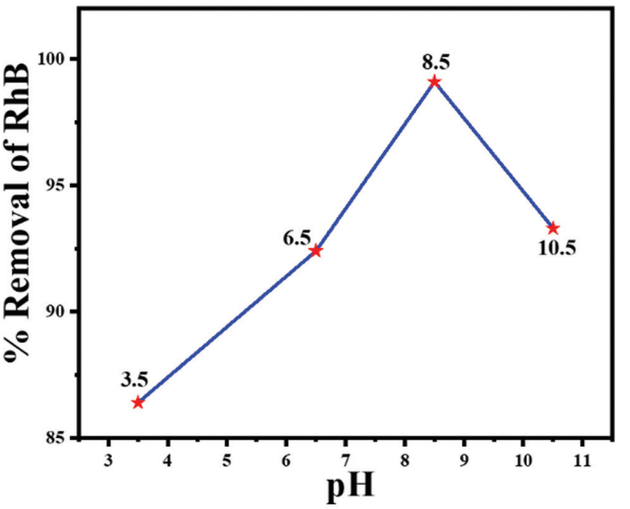

Figure 10. Effect of initial pH on the percentage removal of rhodamine B (RhB) by phosphoric acid-activated carbon. *Maximum removal* occurs at pH 8.5; both acidic and strongly alkaline conditions reduce efficiency.

(b) Optimization of adsorbent dose

The amount of adsorbent used in a batch process is a critical parameter, as it determines the number of available active sites for dye adsorption.[24] In general, increasing the adsorbent dose enhances removal efficiency due to greater surface area and functional group availability.[19]

To determine the optimal quantity of Bc-H for RhB removal, a series of experiments were conducted using four different quantities: 0.02 g, 0.025 g, 0.03 g, and 0.035 g per 100 mL of RhB solution. All other experimental conditions were held constant. The resulting ultraviolet-Vis spectra are shown in Figure 11, and quantitative results are summarized in Table 3.

The data show that RhB removal efficiency improved from 92.3% to 99.9% as the amount increased from 0.020 g to 0.030 g. However, a slight decrease to 97.4% was observed at 0.035 g, which may be attributed to agglomeration of excess adsorbent particles, reducing the effective surface area or causing site overlap.[26]

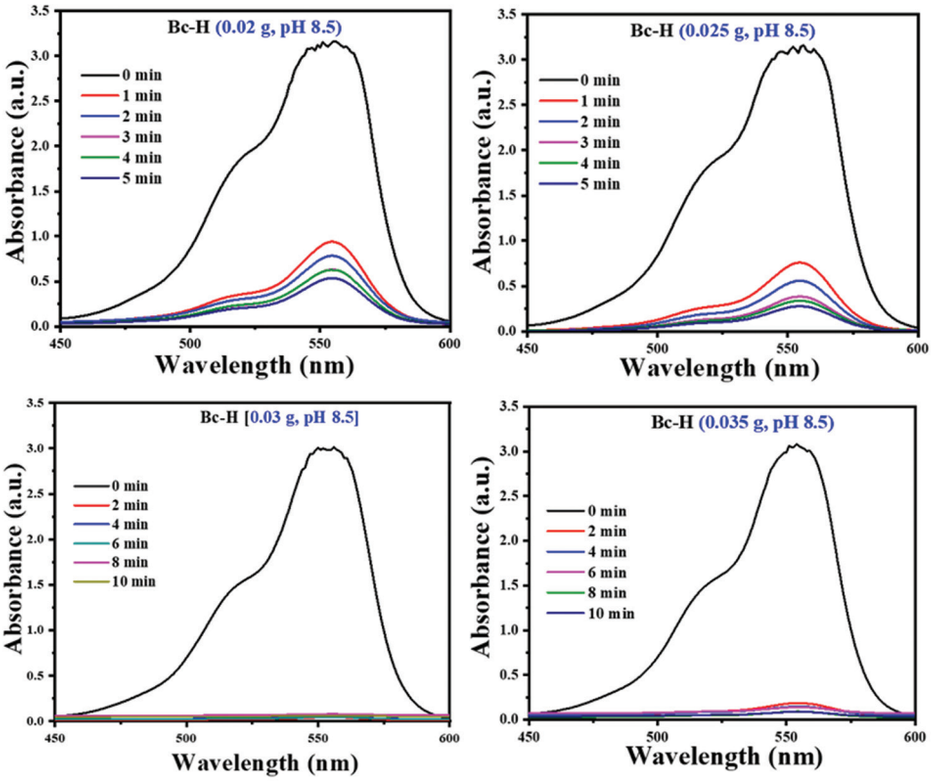

Figure 11. Ultraviolet-vis adsorption spectra of rhodamine B after treatment with varying quantities of phosphoric acid-activated carbon (Bc-H)

Table 3. Effect of phosphoric acid-activated carbon concentration on rhodamine B removal efficiency

Concentration (g/100 mL)	Rhodamine B removal (%)
0.020	92.3
0.025	96.2
0.030	99.9
0.035	97.4

To better visualize performance at high removal levels, a magnified plot of removal percentage versus adsorbent dose is provided in Figure 12.

The optimal dosage of Bc-H for RhB removal was determined to be 0.030 g per 100 mL, balancing high removal efficiency (99.9%) with material economy. Increasing the dose beyond this point offered no additional benefit and may slightly reduce performance due to particle crowding and limited site accessibility.

(c) Contact time studies

Contact time plays a crucial role in determining the adsorption rate and equilibrium behavior of adsorbents. In this study, the effect of contact time was evaluated under optimized conditions (pH 8.5, 0.03 g Bc-H) to assess how quickly the adsorbent can remove RhB from the solution. Among all three ACs, Bc-H demonstrated rapid adsorption kinetics, achieving nearly complete dye removal within just 2 – 4 min. In comparison, Bc-K required significantly more time and showed lower adsorption capacity, while Bc-Na exhibited negligible uptake even after 10 min.

The rapid adsorption observed for Bc-H can be attributed to its high BET surface area, well-developed mesoporous structure, and abundant oxygenated functional groups. These characteristics facilitate efficient dye diffusion, strong electrostatic interactions, and rapid access to active sites.[21] This fast removal profile underscores the suitability of Bc-H for applications requiring real-time or rapid water purification, such as industrial effluent treatment or emergency response scenarios.

3.3.3. Adsorption kinetics and rapid removal efficiency

The adsorption kinetics of RhB onto the synthesized ACs – Bc-H, Bc-K, and Bc-Na – as well as and

commercial AC were evaluated under identical batch conditions (20 ppm RhB, pH 8.5, 0.03 g adsorbent, room temperature). The normalized concentration ratio (C/C_0) was plotted as a function of time to assess the rate and extent of dye removal (Figure 13).

All three synthesized ACs exhibited a rapid initial decrease in C/C_0 within the first 2 min, indicating fast adsorption kinetics. Among them, Bc-H demonstrated the highest performance, achieving >99% RhB removal within just 2 – 4 min. This exceptional efficiency is attributed to its well-developed mesoporosity, high surface area (1,451.2 m^2/g), and the presence of abundant oxygenated surface functional groups, including phosphate-linked moieties, which together promote electrostatic attraction, hydrogen bonding, and π–π interactions with RhB molecules.[27]

The inclusion of commercial AC as a benchmark provides valuable context. As shown in Figure 13, Bc-H (black line) clearly outperformed commercial AC, which achieved approximately 85 – 90% removal after 10 min. Bc-K (blue line) exhibited moderate performance, reaching ~45% removal after 10 min, while Bc-Na (green line) showed negligible adsorption, consistent with its low surface area and poor functionalization.

The limited effectiveness of Bc-K may be attributed to its predominantly microporous structure, which restricts the diffusion of bulky dye molecules, and a relatively low surface area (78.4 m^2/g). Bc-Na's poor performance is likely due to the insufficient activation strength of Na_2CO_3 at 400°C, which resulted in inadequate porosity and minimal functional group development. Furthermore, its alkaline surface chemistry may not favor interaction with cationic RhB molecules.

These observations highlight the critical role of the activation strategy. H_3PO_4 serves as a dehydrating and crosslinking agent, stabilizing the carbon matrix and introducing surface functionalities (–OH, –COOH, –C=O) that enhance adsorption. In contrast, KOH typically requires higher activation temperatures (>700°C) for effective micropore development, and Na_2CO_3 remains ineffective under the moderate thermal conditions used here.

Overall, Bc-H not only surpassed Bc-K and Bc-Na but also exceeded the performance of commercial AC in terms of both adsorption efficiency and rate. Since equilibrium was essentially reached within 2 – 4 min for Bc-H, adsorption isotherm modeling and kinetic fitting were not pursued in the present study. These will be addressed in future investigations across broader concentration and time ranges.

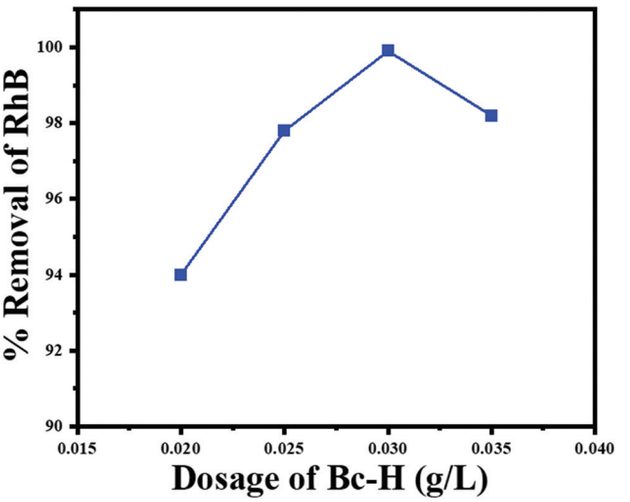

Figure 12. Effect of phosphoric acid-activated carbon (Bc-H) dosage on rhodamine B (RhB) removal efficiency. The y-axis is plotted from 90% to 100% to highlight subtle variations.

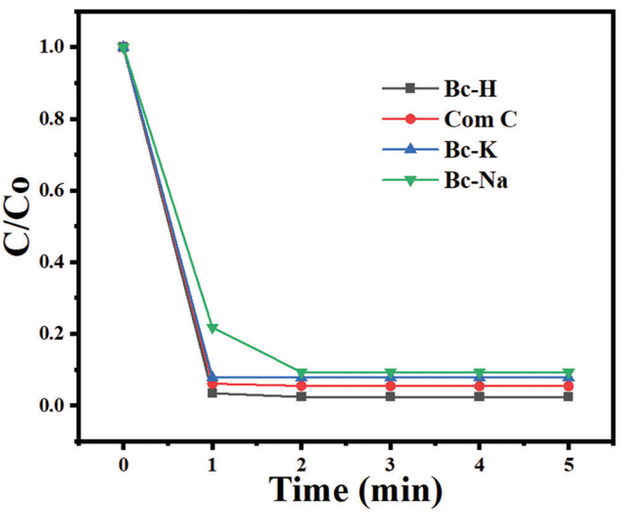

Figure 13. Normalized rhodamine B (RhB) concentration (C/C_0) versus time for Bc-H, Bc-K, Bc-Na, and commercial activated carbon (Com C) under identical conditions (20 ppm RhB, 0.03 g adsorbent, pH 8.5). Bc-H achieved the fastest and most complete dye removal within 2 – 4 min. Bc-H, Bc-K, and Bc-Na refer to acid-activated, base-activated, and salt-activated carbons, respectively.

3.3.4. Quantitative comparison with commercial AC

To provide a clear performance benchmark, Table 4 presents comparative RhB adsorption performance of Bc-H, Bc-K, Bc-Na, and commercial AC under identical conditions.

Bc-H demonstrated the highest removal efficiency and fastest kinetics, achieving 99.9% removal within 2 – 4 min. Commercial AC performed moderately well, reaching ~85 – 90% removal after ~10 min. In contrast, Bc-K and Bc-Na showed limited and negligible adsorption, respectively. These results underscore the superior textural and surface chemical properties of Bc-H, which arise from its high BET surface area, phosphate-linked oxygenated groups, and balanced micro/mesoporous structure.[28,29] These features distinguish Bc-H not only from the other synthesized samples but also from the commercial benchmark.

Although FTIR spectroscopy was used to identify key surface functionalities before dye exposure, post-adsorption spectroscopic analyses (e.g., FTIR, X-ray photoelectron spectroscopy) were not performed. Therefore, the proposed adsorption mechanism – based on electrostatic attraction, hydrogen bonding, and π–π interactions – is supported indirectly by structural and kinetic data. This limitation has been noted, and future studies will include point of zero charge measurements and post-adsorption spectral analysis to provide direct evidence of adsorbent–adsorbate interactions.[30]

The high surface area and well-developed mesoporous structure of Bc-H facilitate rapid dye diffusion, while oxygenated surface groups enhance electrostatic and hydrogen bonding interactions. Furthermore, π–π stacking between the aromatic rings of RhB and graphitic domains in the carbon matrix likely contributes to the strong adsorption affinity.[31]

In addition to its technical merits, Bc-H offers significant economic advantages. The precursor, *B. ceiba* sawdust, is a readily available, low-cost byproduct from sawmills in Nepal. The one-step H_3PO_4 activation at moderate temperature (400°C) minimizes chemical and energy consumption. These factors highlight Bc-H's potential for cost-effective and scalable application, especially in resource-limited regions.

We acknowledge that all samples were carbonized at a fixed temperature of 400°C to isolate the effect of activating agents. However, KOH and Na_2CO_3 may benefit from higher activation temperatures, and future work will explore this variable to optimize textural and adsorptive properties.

3.3.5. Comparison with literature

To further contextualize the performance of Bc-H, Table 5 presents a comparison with RhB adsorption data reported for various biomass-derived adsorbents. While most of the listed adsorbents achieved removal efficiencies above 90%, they generally required higher dosages (0.04 – 0.05 g/100 mL) and longer contact times (30 – 120 min). In contrast, Bc-H removed 99.9% of RhB in just 2 – 4 min at a lower dose (0.03 g), underscoring its outstanding kinetics and practical efficiency.

Table 4. Comparative rhodamine B adsorption performance of carbons under identical conditions

Adsorbent	Brunauer–Emmett–teller surface area (m^2/g)	Rhodamine B removal (%)	Time for~99.9% removal	pH	Dose (g/100 mL)
Bc-H	1,451.2	99.9	2 – 4 min	8.5	0.03
Bc-K	78.4	~45	>10 min	8.5	0.03
Bc-Na	61.2	Negligible	-	8.5	0.03
CAC	989.3	96.4	~6 min	8.5	0.03

Note: Bc-H, Bc-K, and Bc-Na refer to acid-activated, base-activated, and salt-activated carbons, respectively.
Abbreviation: CAC: Commercial activated carbon.

Table 5. Comparison of rhodamine B removal performance between phosphoric acid-activated carbon and other reported biomass-based adsorbents

Adsorbent (Precursor)	Rhodamine B removal (%)	Contact time	Dose (g/100 mL)	Reference
Phosphoric acid-AC (this study)	99.9	2–4 min	0.03	This work
Rice husk biochar	92	60 min	0.05	10
Moringa seed pod AC	94	90 min	0.04	28
Casuarina cone powder	89	120 min	0.05	29
Elaeagnus stone AC	93	30 min	0.05	30

Abbreviation: AC: Activated carbon.

These results confirm that Bc-H not only meets but also exceeds the performance of many reported biomass-based adsorbents, especially in terms of removal speed, dosage efficiency, and practical applicability.

While this study employed FTIR and SEM for surface and morphological analysis, more advanced techniques – such as carbon, hydrogen, nitrogen, and sulfur elemental analysis and transmission electron microscopy – were not included. These will be incorporated in future work to provide a deeper understanding of elemental composition and nanostructure, further enriching the characterization of Bc-H.

4. Conclusion

This study presents a systematic and comparative evaluation of ACs synthesized from *B. ceiba* wood dust using three different chemical activating agents – H_3PO_4, KOH, and Na_2CO_3 – for the adsorption of RhB from aqueous solutions.

Among these, Bc-H consistently exhibited the highest adsorption efficiency, fastest kinetics, and most favorable physicochemical properties. Its superior performance is attributed to its high BET surface area (1,451.2 m^2/g), well-developed mesoporosity, and abundance of surface oxygenated functional groups introduced during H_3PO_4 activation. These features collectively promoted rapid dye diffusion and strong electrostatic, hydrogen bonding, and π–π interactions with RhB molecules. Compared to Bc-K, Bc-Na, and even commercial AC, Bc-H achieved nearly complete RhB removal (>99%) within just 2 – 4 min, highlighting its strong potential for real-time water purification.

Key operational parameters were also optimized. The best performance was observed at pH = 8.5 and an adsorbent dose of 0.03 g/100 mL. In contrast, Bc-K and Bc-Na performed less effectively due to lower surface areas and limited mesoporosity, with Na_2CO_3 showing negligible activation efficiency at the applied temperature.

This work underscores the critical importance of activation strategy in tailoring surface area, porosity, and functional group chemistry for optimal adsorption performance. The one-step H_3PO_4 activation at a moderate temperature (400°C) represents a cost-effective and scalable route for converting *B. ceiba* sawdust – a widely available waste biomass in Nepal – into high-performance AC.

While the current study provides compelling results under batch conditions, it also has a few limitations. Detailed adsorption isotherms (e.g., Langmuir and Freundlich), kinetic modeling (pseudo-first and second-order), and thermodynamic studies were not performed due to the extremely rapid equilibrium behavior observed with Bc-H. In addition, post-adsorption characterization (e.g., FTIR or X-ray photoelectron spectroscopy) and point of zero charge measurements were not included, which limits mechanistic interpretation. Moreover, all adsorption experiments were carried out at room temperature, which restricts understanding of temperature-dependent adsorption behavior and thermodynamic parameters.

To address these gaps, future work will focus on: (i) performing equilibrium isotherm, kinetic, and thermodynamic modeling under broader time and concentration ranges, (ii) investigating the adsorption mechanism in more detail using post-adsorption surface analyses (FTIR, X-ray photoelectron spectroscopy), (iii) exploring variable activation temperatures and impregnation ratios, especially for KOH and Na_2CO_3 activation routes, (iv) evaluating the effect of temperature on adsorption capacity and deriving key thermodynamic parameters (ΔG°, ΔH°, ΔS°), (v) expanding applicability to other classes of pollutants, including heavy metals and emerging contaminants.

The *B. ceiba*-derived AC, particularly Bc-H, offers several notable advantages, such as low-cost synthesis from abundant local biomass, high BET surface area, well-developed mesoporosity, and outstanding RhB removal efficiency. However, certain disadvantages remain. The study was conducted under controlled batch conditions using synthetic dye solutions; thus, its performance under complex real wastewater conditions requires further validation. In addition, the regeneration and reuse of the adsorbent were not evaluated, which is critical for practical field applications. Addressing these aspects will be essential for future scaling and deployment.

In summary, Bc-H emerges as a low-cost, sustainable, and highly effective adsorbent for organic dye removal. Its excellent adsorption capacity, ultrafast kinetics, and eco-friendly synthesis method make it a promising candidate for scalable wastewater treatment, particularly in decentralized or resource-limited settings such as rural areas in Nepal and beyond.

Acknowledgments

The author expresses sincere gratitude to the Institute of Science and Technology (IOST), Central Department of Chemistry, Tribhuvan University, Kirtipur, Nepal; Patan Multiple Campus, Tribhuvan University, Patan Dhoka, Lalitpur; the Global Research Laboratory, Sun Moon

University, South Korea; and Suranaree University of Technology (SUT), Thailand, for their valuable support in carrying out this research.

Funding

None.

Conflict of interest

The author declares no conflict of interest.

Author contributions

This is a single-authored article.

Availability of data

The data supporting the findings of this study are available from the corresponding author upon reasonable request.

References

1. Shrestha D. Efficiency of wood-dust of *Dalbergia sissoo* as low-cost adsorbent for rhodamine-B dye removal. *Nanomaterials (Basel)*. 2021a;11(9):2217. doi: 10.3390/nano11092217
2. Shrestha D. Removal of eosin Y dye using activated carbons from modified wood dust powder of *Dalbergia sissoo*. *Patan Pragya.* 2021b;8(1):57-72. doi: 10.3126/pragya.v8i01.42356
3. Katheresan V, Kansedo J, Lau SY. Efficiency of various recent wastewater dye removal methods: A review. *J Enviorn Chem Engine.* 2018;6(4):4676-4697. doi: 10.1016/j.jece.2018.06.060
4. Al-Gheethi AA, Azhar QM, Kumar PS, *et al*. Sustainable approaches for removing Rhodamine B dye using agricultural waste adsorbents: A review. *Chemosphe.* 2022;287:132080. doi: 10.1016/j.chemosphere.2021.132080
5. Shrestha S, Pradhananga D, Pandey V. *Kathmandu Valley Groundwater Outlook*. Kathmandu, Nepal: Asian Institute of Technology (AIT), The Small Earth Nepal (SEN), Center of Research for Environment Energy and Water (CREEW), International Research Center for River Basin Environment- University of Yamanashi (ICRE-UY); 2012.
6. Yadav SN, Rai S, Behera M, *et al*. Dynamic assembly and stabilization of surfactant-dye-polyelectrolyte complexes: An overview. *J Mol Liq.* 2025;421:126897. doi: 10.1016/j.molliq.2025.126897
7. Rokaya MB, Parajuli B, Timsina B. Vegetation and forest in Nepal. In: *Flora and Vegetation of Nepal*. Cham: Springer International Publishing, 2024. p. 37-88. doi: 10.1007/978-3-031-50702-1_3
8. Saigl ZM. Various adsorbents for removal of rhodamine b dye: A review. *Indones J Chem.* 2021;21(4):1039-1056. doi: 10.22146/ijc.62863
9. Smith RT, Brown LM, Davis PK. Impact of synthetic dyes on aquatic ecosystems. *Wat Resear.* 2020;185:116250. doi: 10.56557/upjoz/2023/v44i133542
10. Ding L, Zou B, Gao W, *et al*. Adsorption of Rhodamine-B from aqueous solution using treated rice husk-based activated carbon. *Colloids Surf A Physicochem Eng Asp.* 2014;446:1-7. doi: 10.1016/j.colsurfa.2014.01.030
11. Li Z, Xu M, Xia Y, *et al*. High-frequency supercapacitors surpassing dynamic limit of electrical double layer effects. *Nat Commun*. 2025;16:3704. doi: 10.1038/s41467-025-59015-7
12. Dutta S, Gupta B, Srivastava S, Gupta A. Recent advances on the removal of dyes from wastewater using various adsorbents: A critical review. *Mater Advan.* 2021;14(2):4497-4531. doi: 10.1039/D1MA00354B
13. Mondal S, Purkait MK, De S. *Advances in Dye Removal Technologies*. Singapore: Springer; 2018. p. 323. doi: 10.1007/978-981-10-6293-3
14. Ruan W, Hu J, Qi J, Hou Y, Zhou C, Wei X. Removal of dyes from wastewater by nanomaterials: A review. *Adv Mater Lett*. 2019;10(1):9-20. doi: 10.5185/amlett.2019.2148
15. Dassanayake RS, Acharya S, Abidi N. Recent advances in biopolymer-based dye removal technologies. *Molecules.* 2021;26(15):4697. doi: 10.3390/molecules26154697
16. Shindhal T, Rakholiya P, Varjani S, *et al*. A critical review on advances in the practices and perspectives for the treatment of dye industry wastewater. *Bioengineered.* 2021;12(1):70-87. doi: 10.1080/21655979.2020.1863034
17. Samsami S, Mohamadizaniani M, Sarrafzadeh MH, Rene ER, Firoozbahr M. Recent advances in the treatment of dye-containing wastewater from textile industries: Overview and perspectives. *Proc Safe Environ Protect.* 2020;143:138-163. doi: 10.1016/j.psep.2020.05.034
18. Cai Z, Sun Y, Liu W, Pan F, Sun P, Fu JM. An overview of nanomaterials applied for removing dyes from wastewater. *Environ Sci Pollut Res.* 2017;24:15882-15904. doi: 10.1007/s11356-017-9003-8
19. Geçgel Ü, Üner O, Gökara G, Bayrak Y. Adsorption of cationic dyes on activated carbon obtained from waste Elaeagnus stone. *Adsorpt Sci Technol*. 2016;34:512-525. doi: 10.1177/0263617416669727
20. Xiao W, Garba Z, Sun S, *et al*. Preparation and evaluation of an effective activated carbon from white sugar for

the adsorption of rhodamine B dye. *J Clean Prod*. 2020;253:119989.
doi: 10.1016/j.jclepro.2020.119989

21. Laasri L, Elamrani MK, Cherkaoui O. Removal of two cationic dyes from a textile effluent by filtration-adsorption on wood sawdust. *Environ Sci Pollut Res Int.* 2007;14:237-240.
doi: 10.1065/espr2006.08.331
22. Pourabadeh A, Baharinikoo L, Nouri A, Mehdizadeh B, Shojaei S. The optimisation of operating parameters of dye removal: Application of designs of experiments. *Inter J Environ Anal Chem.* 2021;101(9):1320-1329.
doi: 10.1080/03067319.2019.1680657.
23. Lacerda VD, López-Sotelo JB, Correa-Guimarães A, *et al*. Rhodamine B removal with activated carbons obtained from lignocellulosic waste. *J Environ Manag*. 2015;155:67-76.
doi: 10.1016/j.jenvman.2015.03.007.
24. Inyinbor AA, Adekola FA, Olatunji AG. Adsorption of Rhodamine B dye from aqueous solution on *Irvingia gabonensis* biomass: Kinetics and thermodynamics studies. *S Afr J Chem.* 2015;68:115-125.
doi: 10.17159/0379-4350/2015/v68a17
25. Dahri MK, Kooh MRR, Lim LBL. Remediation of rhodamine B Dye from aqueous solution using *Casuarina equisetifolia* cone powder as a low-cost adsorbent. *Adv Phys Chem.* 2016;9497378.
doi: 10.1155/2016/9497378
26. Lim LBL, Priyantha N, Fang XY, Mohamad Zaidi NAH. *Artocarpus odoratissimus* peel as a potential adsorbent in environmental remediation to remove toxic Rhodamine B dye. *J Mater Environ Sci*. 2017;8:494-502.
27. Bello OS, Lasisi BM, Adigun OJ, Ephraim V. Scavenging rhodamine B dye using *Moringa oleifera* seed pod. *Chem Speciat Bioavailab*. 2017;29:120-134.
doi: 10.1080/09542299.2017.1356694
28. Rasapoor M, Young B, Asadov A, *et al*. Effects of biochar and activated carbon on biogas generation: A thermogravimetric and chemical analysis approach. *Energy Convers Manag.* 2020;203:112221.
doi: 10.1016/j.enconman.2019.112221
29. Senturk HB, Ozdes D, Duran C. Biosorption of Rhodamine 6G from aqueous solutions onto almond shell (*Prunus dulcis*) as a low cost biosorbent. *Desalination*. 2010;252:81-87.
doi: 10.1016/j.desal.2009.10.021
30. Wang J, Zhou Y, Liu X. Adsorption techniques for dye removal from wastewater: A review. *Environ Sci Pollut Res.* 2019;26(1):1-15.
31. Johnson AB, Lee CD. Toxicity of rhodamine B dye in aquatic environments. *Environ Toxico Chem*. 2018;37(5):1200-1210.